Hindawi
Advances in Materials Science and Engineering
Volume 2021, Article ID 4921365, 14 pages
https://doi.org/10.1155/2021/4921365

*Research Article*

# Study on the Freeze-Thaw Process of the Lining Structures of a Tunnel on Qinghai-Tibet Plateau with the Consideration of Lining Frost Damage

**Hong Yu**,[1,2] **Kun Zhang**,[3] **Xiaoming Zhu**,[4] **Zhizhuo Tian**,[3] **and Qinglong Zhang**[3]

[1]*Gansu Province Highway Traffic Construction Group Co., Ltd., Lanzhou 730030, China*
[2]*State Key Laboratory of Frozen Soil Engineering, Northwest Institute of Eco-Environment and Resources, Chinese Academy of Sciences, Lanzhou 730000, China*
[3]*Gansu Provincial Transportation Research Institute Group Co., Ltd., Lanzhou 730000, China*
[4]*Gansu Province Transport Planning Survey & Designing Institute Co., Ltd., Lanzhou 730030, China*

Correspondence should be addressed to Kun Zhang; zhangkun2020@163.com

Received 6 May 2021; Accepted 24 June 2021; Published 8 July 2021

Academic Editor: Hao Zheng



In seasonally frozen ground, there are many frost problems in highway road tunnel after its excavation due to the heat exchange between the cold air and lining structure inside the tunnel. To mitigate these frost-related damages, thermal insulation layer is widely used at entrance and exit sections of the tunnel. In this study, a coupled mathematical model of heat, moisture, and stress was built for tunnels in seasonally permafrost regions. Then, based on the field-observed air temperature inside a roadway tunnel at Altun Mountain on the Qinghai-Tibet Plateau (QTP), seasonal freeze-thaw process of the surrounding rocks (SR) and lining structures were numerically investigated with the consideration of insulation methods: without insulation (WTIL) and laying the insulation layer on the inner surface of the second lining structure (STIL). Combined with the principle of Miner damage accumulation, the stress regimes of the lining structures of tunnel were investigated in WTIL and STIL. The results show that there was a significantly thermal disturbance of the SR after the tunnel excavation. In the 5$^{th}$ year of the operation period, the maximum seasonal freeze depth (MSFD) of the SR can reach 1.6 m at the vault of the arch and that at the inverted arch was only 1.0 m due to the pavement inside the tunnel. Then, both the absolute maximum value of the maximum principal stress (MAPS) and minimum principal stress (MIPS) in cold season were bigger than those in warm season comparing the value of the stress filed of the lining structure. In the same way, both the MAPS and MIPS of the lining structure in WTIL are bigger than those in STIL in numerical simulation. The positions of the maximum tensile stress of the primary lining structure in STIL and WTIL were inverted arch. For the lining structures, the greater tensile stress was generally harmful. Thus, the inverted arch of the tunnel should be laid on the insulation layer.

## 1. Introduction

Frozen ground is defined as soil or rock including ice with a temperature at or below 0°C, which can be divided into permafrost and seasonal permafrost [1]. In China, permafrost regions and seasonally frozen regions account for about 20% and 55% of the total land area, which are mainly distributed in the western, northeastern China, and Qinghai-Tibet Plateau [1–6]. In recent years, more and more engineered infrastructures were built in seasonally frozen regions of China. Highway tunnels, as one of the common engineered structures, are commonly affected by the frost damage [7, 8]. After the excavation, the temperature, stress, and even water fields of SR change due to the heat exchange between the lining structure and the air inside the tunnel [8–11]. As we known, the physical and mechanical properties of frozen soils (rocks) are connected closely to their temperature conditions and moisture contents. Hence, with the changes in temperature and moisture fields, the mechanical properties of frozen soils will also change

significantly. For the tunnels in seasonally frozen regions, there are frost deformations and moisture migrations in the SR due to the heat exchange with the cold air in winter, leading to deformation, cracking, and destruction of the lining structure [9–11]. The problems related to freezing of the lining structures and SR generally seriously affect the safe operation and the traffic of the tunnel. Engineering practices indicated that the frost damage to the tunnels in seasonally frozen regions was serious and common [12]. Thus, it is necessary to study the frost damage mechanisms and prevention methods to the tunnels in seasonal frozen regions.

To mitigate frost related damage, thermal insulation is widely used at entrance and exit section of the tunnels. Moreover, the study methods of the frost damage problems including filed test measurement, evaluation method, and numerical simulation are widely used to gain the factors thermal insulation design needed. Since 1963, Johansen et al. [13] carried out long-term observations of air-temperature beside a tunnel near the Alaska and gained the distribution of air temperature beside the tunnel. Through the field test measurement of a tunnel in cold environment, Okada and Matsumoto [14] studied the day variation of air temperature and the maximum frozen depth inside the tunnel. Nie [15] observed the air temperature inside and outside a seasonal frost tunnel in Daxing'anling Mountain, Northeast of China. The results showed that the part length of variation rate of air temperature inside the tunnel occupied 1/2 of the whole length of the tunnel. Lai et al. [16] studied the difference of the air temperature inside Daban Mountain tunnel, a road tunnel in Qinghai province, under the conditions of thermal insulation gate set in the entrance and exit of the tunnel. The results showed that the thermal insulation effect of installation of the thermal insulation door was better than that of installation of the snow shelter. Based on the results of field test measurement, the temperature, stress, and moisture fields of the SR and lining structures could be investigated according to the conservation law of mass and energy. In 1973, the Harlan model proposed by Harlan was widely used in the permafrost engineering, which could describe the coupling effect of the moisture migration and temperature flux [17]. Based on the Clapeyron equation and Kelvin equation, Shingo [18] studied the force power of the liquid water migration. Taylor and Luthin [19] proposed a coupling model with the consideration of moisture and temperature in freezing process of the soils according to the Harlan model. Shoop and Bigl [20] used the simulation methods of the coupling model of moisture and temperature to investigate the results of a large-scale freeze-thaw test. Hansson et al. [21] proposed a coupling model of moisture and temperature based on the Richards equation and the model validity was demonstrated combined the comparison of the simulated and freezing test results. Based on the above theories and observed data, many scholars studied insulation methods and the freeze-thaw process of lining and SR. Using heat transfer theory and percolation theory, Lai et al. [22] proposed the coupling model with the consideration of the temperature, moisture, and stress of the lining and SR inside the tunnel. Combined the Galiaojin method, the calculation formula of this model could be gained, which was widely used in related studies of seasonal frozen tunnels. Zhang et al. [23] studied the freeze-thaw process of SR inside a seasonal frozen tunnel under the conditions of different construction seasons, different initial temperatures, and different insulation materials using finite element methods. With the consideration of the wind filed inside the tunnel, Tan et al. [24] investigated the temperature filed of SR inside the tunnel, Galongla tunnel on the QTP, under the conditions of different wind speeds and temperatures. Zhou et al. [25] established a mathematical optimization model with the consideration of the factors including insulation parameters, tunnel depth, and economic costs. Ma et al. [26] analyzed the insulation effect of different insulation thicknesses and laying positions and established the relationship between the insulation effect and the thicknesses. Combining Plath's equation and Fourier integral transform, Liu et al. [27] studied the temperature filed of a tunnel in cold environment under the conditions of different convective heat transfer coefficients, different insulation thicknesses, and different initial temperatures.

In this paper, the Altun Mountain highway tunnel was taken as the research object. In order to observe the air temperatures inside the tunnel, corresponding measurement sensors and a weather station were installed inside and outside the tunnel. According to the design of Altun Mountain highway tunnel, geological survey report, and monitoring meteorological data, a coupling model considering the damage of tunnel lining structure was established. With the model, the distribution of temperature field of surrounding rock body under different insulation laying methods was systematically studied by using numerical method. Under the different methods, the temperature field of SR and the stress field of lining were compared and analyzed with the equivalent indoor experimental freeze-thaw damage model. It is hoped that the filed observations and numerical simulations in this study would provide references for thermal insulation design of tunnels built in seasonally frozen regions.

## 2. Mathematical Model and Governing Equations

*2.1. Liquid Water Flows.* Based on the law of mass conservation, the equivalent volume of water content $\theta$ without the consideration of water vapor and salt migration in freeze-thaw soils can be written as [5, 21, 28]

$$\frac{\partial \theta}{\partial t} = \frac{\partial \theta_u}{\partial t} + \frac{\rho_i}{\rho_w}\frac{\partial \theta_i}{\partial t} = \nabla\left(q_{lh} + q_{lT}\right), \tag{1}$$

where $\theta$, $\theta_u$, and $\theta_i$ are the equivalent volume of water, unfrozen water, and ice content, respectively ($m^3 \cdot m^{-3}$); $\rho_i$ and $\rho_w$ are the density of ice and water ($kg \cdot m^{-3}$); $t$ is the time; and $q_{lh}$ and $q_{lT}$ are the liquid water flux density related to pressure head gradient and temperature gradient, respectively ($m \cdot s^{-1}$).

Based on thecHarlan model, there is a similar law of liquid water migration in frozen and unfrozen unsaturated soil, which can be described by Richard equation [1, 17]. In a

previous study, the regulation law of liquid water migration in freeze-thaw soils can be assumed to Darcy's law [5, 29]. The flux density of liquid water under the potential gradient in freeze-thaw soil can be written as [5, 17, 21, 28, 29]

$$q_{lh} = -K_{lh}\nabla(h + y), \tag{2}$$

where $y$ is the vertical coordinate (m); $h$ is the pressure head of liquid water in freeze-thaw soils (m); and $K_{lh}$ is the water conductivity coefficient of liquid water under potential gradient in freeze-thaw soils ($m{\cdot}s^{-1}$). The liquid water flux density $q_{lT}$ related to temperature gradient can be written as

$$q_{lT} = -K_{lT}\nabla(T), \tag{3}$$

where $K_{lT}$ is the water conductivity coefficient related to temperature gradient ($m^2{\cdot}K^{-1}{\cdot}s^{-1}$), which can be written as

$$K_{lT} = K_{lh}\left(hG_{wT}\frac{1}{\gamma_0}\frac{d\gamma}{dT}\right),$$
$$\gamma = 75.6 - 0.1425T - 2.38 \times 10^{-4}T^2, \tag{4}$$

where $G_{wT}$ is gain factor, which can evaluate the temperature effect due to the surface tension of solid granule; $\gamma$ is surface tension of the solid granule; and $\gamma_0$ is the surface tension of the solid granule at 25°C (approximately $71.89\,g{\cdot}s^{-2}$). Then, the mass conservation equation of liquid water in freeze-thaw soil can be written as [5, 30]

$$\frac{\partial\theta}{\partial t} = \nabla\cdot\left[K_{lh}\nabla(h + y) + K_{lT}\nabla(T)\right]. \tag{5}$$

Soil-water characteristic curve (SWCC) can describe the connection between liquid water and energy in freeze-thaw soil. Based on a previous study, the relationship among matric, volume water content, and saturation in freeze-thaw soils also can be described by SWCC [29]. In this study, the hydraulic properties of unsaturated freeze-thaw soil based on van Genuchten model and Mualem model can be written as [30, 31]

$$h = \frac{-\left(S_e^{(1/-m)} - 1\right)^{(1/n)}}{\alpha},$$
$$S_e = \frac{\theta_l - \theta_r}{\theta_s - \theta_r} = \begin{cases} \dfrac{1}{\left[1 + |\alpha h|^n\right]^m}, & h < 0, \\ 1, & h \geq 0, \end{cases}$$
$$K = \begin{cases} K_s S_e^i\left[1 - \left(1 - S_e^{(1/m)}\right)^m\right]^2, & h < 0, \\ K_s, & h \geq 0, \end{cases} \tag{6}$$

where $S_e$ is effective saturation of soils; $K_s$ is saturation water conductivity coefficient ($m{\cdot}s^{-1}$); $\theta_l$, $\theta_s$, and $\theta_r$ are liquid water, saturated liquid water, and residual water content, respectively ($m^3{\cdot}m^{-3}$); $\alpha$ is the derivative of the soil intake value ($m^{-1}$); and $n$ and $l$ are experience parameters and $m = 1 - 1/n$ [31].

*2.2. Heat Transfer.* With the considerations of the convection, phase change of ice-water and liquid water migration, heat transfer during the transient flow in freeze-thaw soils can be written as [1, 3–5, 17, 21, 28, 29]

$$C\frac{\partial T}{\partial t} = \frac{\partial}{\partial x}\left(\lambda\frac{\partial T}{\partial x}\right) + \frac{\partial}{\partial y}\left(\lambda\frac{\partial T}{\partial y}\right) + L\rho_i\frac{\partial\theta_i}{\partial t} + C_w\nabla\left[\left(K_{lh}\nabla(h + y) + K_{lT}\nabla T\right)T\right], \tag{7}$$

where $C$ is volume heat capacity; $\lambda$ is thermal conductivity; and $L$ is the latent heat of freezing of liquid water (approximately $3.34 \times 10^5\,J{\cdot}kg^{-1}$).

In freeze-thaw soils, a part of liquid water can exist even at a very low temperature, which is unfrozen water. In previous studies, the empirical expression as follows is used to describe the variation of maximum unfrozen water content $\theta_{u\max}$ under low temperatures in freeze-thaw soils [1, 3–5, 28, 29]:

$$\theta_{u\max} = a(T - 273.15)^{-b}, \tag{8}$$

where $a$ and $b$ are experimental parameters. Then, based on the law of conservation of mass, the volume liquid water content $\theta_l$ can be written as [5, 28, 29]

$$\theta_l = \begin{cases} \theta, & \text{others}, \\ \theta_{u\max}, & T < T_f \text{ and } \theta > \theta_{u\max}, \end{cases} \tag{9}$$

where $T_f$ is the freezing point of the soil, which is assumed to be 0°C in this study. Based on a previous study, the freezing point of soil should be a temperature value where ice starts to grow [32].

*2.3. Mechanism Equation.* Based on the theory of linear momentum balance, the equation of linear momentum in the lining structures and SR can be written as [8]

$$\sigma_{ij,j} + \rho f_i = \rho\frac{dV_i}{dt}, \tag{10}$$

where $\sigma_{ij}$ is the component of stress tensor; $\rho$ is the density; and $f_i$ is the component of volume force. Only with the consideration of the gravity in volume force, $f_i$ can be written as

$$f_i = g_i = (0, 0, g)^T, \tag{11}$$

where $g$ is the acceleration of gravity (approximately $9.8\,m/s^2$).

Combining equation (10) with equation (11), the equation of static equilibrium in the lining structure and SR can be described as

$$\sigma_{ij,j} + \rho f_i = 0. \tag{12}$$

Based on the previous studies and theories related to the linear thermal stress, the elastic deformation displacement and stress produced by external force can be superposed with those produced by the temperature action algebraically. Hence, combined the theory of elastic mechanics, the stress in the lining structure and SR can be written as

$$\varepsilon = \varepsilon_{ij}^{e} + \varepsilon_{ij}^{T} + \varepsilon_{ij}^{i}, \tag{13}$$

where $\varepsilon$ is the stress in the lining structure and SR; $\varepsilon_{ij}^{e}$ is the increment of elastic stress; $\varepsilon_{ij}^{T}$ is the increment of heat stress produced by the temperature action; and $\varepsilon_{ij}^{i}$ is the increment of stress produced by the frost expansion due to ice-water phase change and liquid water migration, which can be described as [6]

$$\varepsilon_{ij}^{i} = 0.09(\theta - \theta_w) + (\theta - n). \tag{14}$$

The elastic constitutive equation in lining structure and SR can be written as

$$\sigma_{ij} = C_{ijkl}^{e}\left(\varepsilon_{kl} - \varepsilon_{kl}^{T} - \varepsilon_{ij}^{i}\right) = C_{ijkl}^{e}\left[\varepsilon_{kl} - \beta_s(T_s - T_{s0})\delta_{kl} - \varepsilon_{ij}^{i}\right], \tag{15}$$

where $T_s$ and $T_{s0}$ are the temperatures of the lining structure and SR and reference temperature (approximately 20°C), respectively; $\beta_s$ is coefficients of linear thermal expansion of the lining structure and SR; and $C_{ijkl}^{e}$ is the elasticity matrix. Combining equation (12) with equation (15), it can be gained as follows:

$$\left[C_{ijkl}^{e}\varepsilon_{kl}\gamma(T_s - T_{s0})\delta_{ij} - \varepsilon_{ij}^{i}\right]_{,j} + \rho f_i = 0. \tag{16}$$

It is assumed that the deformation of the lining structure and SR are all small deformations. Hence, based on the elastic mechanics, the geometric equation of lining structure and SR can be written as

$$\mathrm{d}\varepsilon_{ij} = \frac{1}{2}\left(\frac{\partial \mathrm{d}u_i}{\partial x_j} + \frac{\partial \mathrm{d}u_j}{\partial x_i}\right), \tag{17}$$

where $\varepsilon_{ij}$ is the component of stress tensor and $u_i$ is the component of the deformation. Combined with equation (16), the mechanism equation of lining structure and SR can be written as

$$\left[\frac{1}{2}C_{ijkl}^{e}\left(\frac{\partial \mathrm{d}u_i}{\partial x_j} + \frac{\partial \mathrm{d}u_j}{\partial x_i}\right) - \gamma_s(T_s - T_{s0})\delta_{ij} - \varepsilon_{ij}^{i}\right]_{,j} + \rho f_i = 0. \tag{18}$$

According to previous and related studies, the equivalent elastic modulus $E$ and equivalent poison's ratio $\nu$ of the SR in freezing and thawing processes can be written as [33]

$$E = \frac{[c_sE_s(1-2\nu_i) + c_iE_i(1-2\nu_s)][c_sE_s(1+\nu_i) + c_iE_i(1+\nu_s)]}{c_sE_s(1-2\nu_i)(1+\nu_i) + c_iE_i(1-2\nu_s)(1+\nu_s)},$$

$$\nu = \frac{c_sE_s\nu_s(1-2\nu_i)(1+\nu_i) + c_iE_i\nu_i(1-2\nu_s)(1+\nu_s)}{c_sE_s(1-2\nu_i)(1+\nu_i) + c_iE_i(1-2\nu_s)(1+\nu_s)}, \tag{19}$$

where $c_s$ and $c_i$ are the volume contents of the solid granule and ice, respectively.

## 3. A Tunnel Built on the Qinghai-Tibet Plateau

*3.1. Study Area and Tunnel.* In this study, a highway tunnel on the QTP was used to study the freeze-thaw process of the lining structure of tunnels in seasonal frost regions. The study area is located at southeast edge of the QTP, with an elevation above 3000 m. According to Lenghu weather station closet to this site, the mean annual air temperature is about 3.6°C, and the maximum and minimum air temperatures are 26.9 and −21.7°C in past 10 years, respectively (Figure 1). Meanwhile, this engineering site is in an alpine and semi-arid climate zone, with a little annual precipitation.

*3.2. Air Temperature Observation along the Tunnel.* The tunnel on the QTP has a length of 7,527 m and faces potential frost damage according to the air temperature data monitored by Lenghu weather station. In previous studies, the section closest to the entrance of the tunnel generally suffers worst frost damage. To gain the variation of air temperature at that entrance (D1) of the tunnel (Figure 2), an air temperature sensor was placed at 5 m from the entrance. The sensor used in this monitoring test was manufactured and calibrated by TASCO (Japan), with a calibrated range from −30 to 60°C and a resolution smaller than 1.0°C. The date acquisition of air temperature was set as 4 hours.

## 4. Numerical Simulations

*4.1. Computational Model.* Based on previous studies and related works, the boundary error in numerical simulations would be less than 10% when the computational domain is 3–5 times of the equivalent diameter of the tunnel [5, 34]. Then, the computational model was constructed based on the actual section D1 of the tunnel in this study (Figure 3). The insulation methods were considered in this study: without insulation (WTIL) and laying the insulation layer on the inner surface of the second lining structure (STIL).

According to the geological survey conducted, the SR at D1 section of tunnel can be simplified as one kind material. The thermal and hydraulic parameters of the SR and lining structure are listed in Table 1, which were gained based on the borehole drilling, related laboratory tests, and previous studies [1, 17, 21, 28, 29].

For the lining structures of tunnel in seasonal frost regions, the effect of freeze-thaw circle is one of main factors affecting the mechanical properties of lining structures. At present, although massive rapid freeze-thaw test data of concrete have been accumulated, it was still considerably

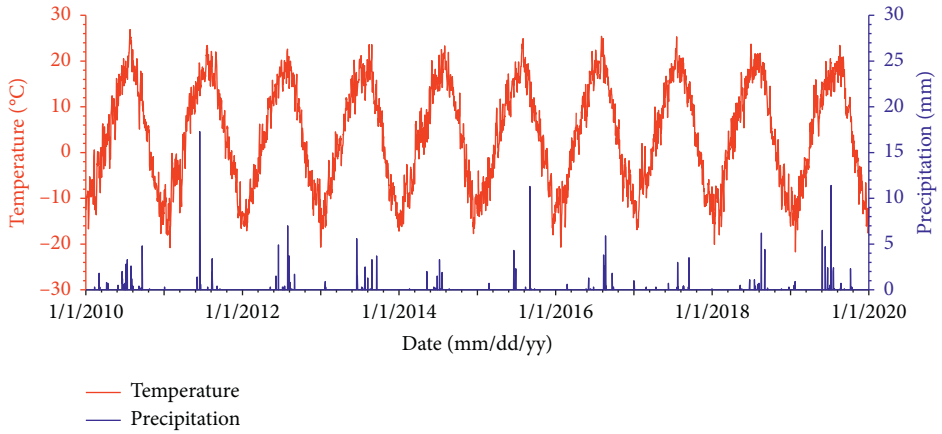


Figure 1: Observation of air temperature and precipitation in the study area monitored by Lenghu weather station.

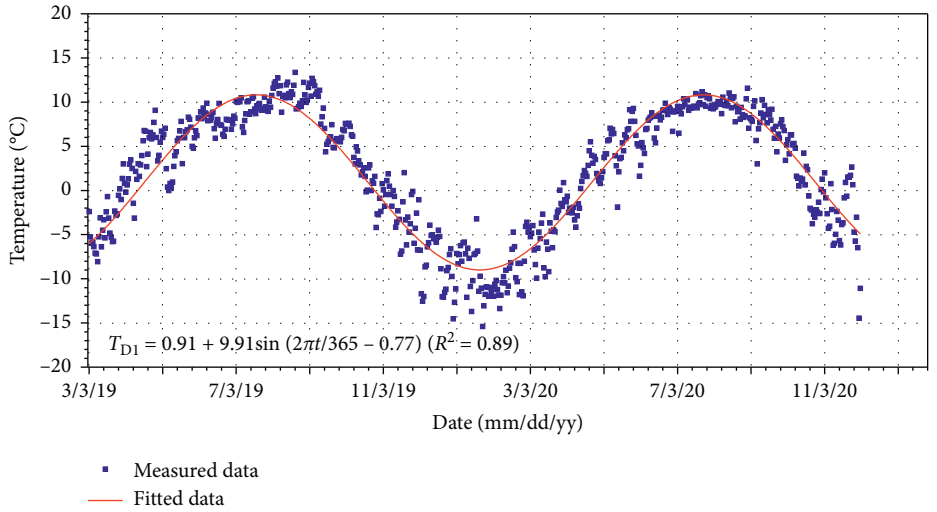


Figure 2: Observation of air temperature at D1 inside the tunnel monitored with a temperature sensor.

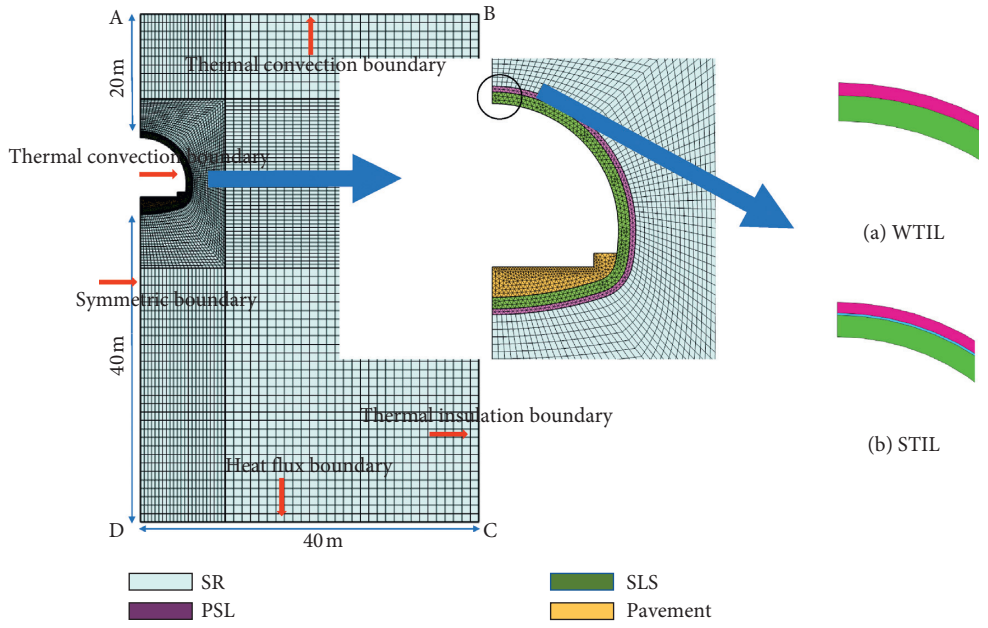


Figure 3: Numerical model of the Altun mountain tunnel.

Table 1: Thermal and hydraulic parameters of lining structures, insulation layer, and SR in the simulation.

| Parameters | $\lambda_u$ W/(m·°C) | $\lambda_f$ W/(m·°C) | $C_u$ J/(kg·°C) | $C_f$ J/(kg·°C) | $a$ | $b$ | $\alpha$ ($m^{-1}$) | $\theta_r$ | $\theta_s$ | $K_s$ ($m \cdot s^{-1}$) | $\rho$ ($kg \cdot m^{-3}$) | $L_s$ ($J \cdot m^{-3}$) |
|---|---|---|---|---|---|---|---|---|---|---|---|---|
| PLS | 2 | 2 | $2.30 \times 10^6$ | $2.30 \times 10^6$ | — | — | — | — | — | — | 2500 | — |
| SLS | 2 | 2 | $2.30 \times 10^6$ | $2.30 \times 10^6$ | — | — | — | — | — | — | 2500 | — |
| TIL | 0.037 | 0.037 | $9.40 \times 10^5$ | $9.40 \times 10^5$ | — | — | — | — | — | — | 188 | — |
| SR | 1.47 | 1.82 | $2.09 \times 10^6$ | $1.84 \times 10^6$ | 9.3 | 0.52 | 2.3 | 0.02 | 0.25 | $1.2 \times 10^{-8}$ | 1700 | $3.77 \times 10^7$ |

difficult to apply in practical prediction of concrete durability and freeze-thaw damage due to the great differences of freeze-thaw between in actual and lab environments. In previous studies and related works, based on the principle of Miner damage accumulation, Liu and Tang established a calculation expression of equivalent lab freeze-thaw cycles of concrete by comparing and analyzing the difference and relation between the actual and lab environments [35]. Then, the expression of equivalent freeze-thaw cycles $N_{\text{eq}}$ in lab tests of concrete can be written as

$$N_{\text{eq}} = \left( \sum_i \frac{N_i}{N_{Fi}} \right) N_F = \left( \sum_i \frac{N_i}{\kappa_i^{-\xi} N_F} \right) N_F = \sum_i \kappa_i^{\xi} N_i, \quad i = 1, 2, \ldots, \tag{20}$$

where $N_{\text{eq}}$ is the equivalent freeze-thaw cycles in lab tests of concrete; $N_1$ is the number of freeze-thaw cycles in actual environment of concrete; $N_{F1}$ is the fatigue life under different freeze-thaw cycles in actual environment of concrete; $\kappa_i$ is the proportional coefficient between hydrostatic pressures in lab and actual environments; and $\xi$ is a material parameter related to concrete (approximately 0.946), which is a constant under the assumption that the properties of concrete materials do not change with the freeze-thaw environment [36]. Based on previous studies and related works, $\kappa_i$ can be written as

$$\kappa_i \approx \frac{\dot{T}_i}{\dot{T}} \approx \frac{T_i / t}{T / t_2}, \tag{21}$$

where $\Delta T_i$ is the difference between daily maximum air temperature and minimum temperature in actual environment; $t_1$ is the time interval between daily maximum air temperature and minimum temperature in actual environment; $\Delta T$ is the difference between maximum air temperature and minimum temperature in lab environment; and $t_2$ is the time interval between daily maximum air temperature and minimum temperature in lab environment. In previous studies, $\Delta T / t_2$ is approximately 12.5°C/h [37]. Based on the measured air temperature data in this study, $\kappa_i$ can be calculated using equation (21), as shown in Table 2. Meanwhile, the equivalent freeze-thaw cycles in lab tests of concrete (EFTC) of this tunnel is 0.92 $1/y$ in actual environment with WTIL.

But for STIL, the EFTC of the lining structure would be smaller with the effect of insulation layer. Due to the limited of actual site operation, there was no temperature sensor laying in the lining structure of the tunnel. Then, based on the measured air temperature, the EFTC with STIL can be gained using numerical simulation in this study.

According to the construction instructions of the tunnel, a 5 cm thick insulation material was laid with STIL. In numerical simulation, the thermal conductivity and specific heat capacity of insulation layer were set as 0.025 W/(m·°C) and 5000 kg·°C, respectively. Based on measured air temperature, the maximum air temperature at D1 section was 17.3°C and the minimum was −17.5°C. Using equation (21), $k_i$ was 2.9 under most unfavorable situation. In numerical simulation, the inner surface of TIL with STIL was set as convection heat transfer boundary and the air temperature can be written as

$$T_{\text{air}} = \begin{cases} \dfrac{34.8t}{12} - 17.3, & 0 \le t \le 12\,\text{h}, \\ -\dfrac{34.8\,(t - 12)}{12} + 17.5, & 12\,\text{h} \le t \le 24\,\text{h}. \end{cases} \tag{22}$$

Based on the simulation results, it could be found that the temperature of the inner surface of the TIL is basically the same as the air temperature after the whole freeze-thaw cycle, while the change of inner surface of the second lining structure is much smaller than that of inner surface of TIL (Figure 4). Meanwhile, the EFTC of the second lining structure (SLS) under STIL was 0.17 $1/y$ using equation (21).

Based on previous studies and related works, the relationship between the dynamic elastic modulus and time of concrete can be written as [38]

$$\begin{aligned} E_{n1} &= -7.07 + 3.54e^{(n/59.89)} + 3.54e^{(n/73.20)} \left(R^2 = 0.99\right), \\ E_{n2} &= -5.16 + 2.58e^{(n/84.38)} + 2.58e^{(n/103.13)} \left(R^2 = 0.97\right), \end{aligned} \tag{23}$$

where $E_{n1}$ and $E_{n2}$ are the dynamic elastic modulus of primary lining structure (PLS) and second lining structure (SLS), respectively, and $n$ is the number of freeze-thaw cycles in lab environment. In this study, the physical parameters in numerical simulation are listed in Table 3.

*4.2. Boundary Conditions.* The thermal boundary conditions of the tunnel in the numerical simulation were determined as follows. The upper boundary AB and the inner wall of the tunnel were set as heat convection boundary. According to the geothermal gradient beneath the tunnel, the heat flux at CD was 0.03 $W/m^2$. The lateral boundary BC was thermal insulation boundary and AD was the symmetry boundary. The water boundary conditions were determined as follows. The boundaries AB, BC, and CD were set as waterproof boundaries without the consideration of rainfall on the water content of SR. The boundary AD was also set as symmetry boundary. The stress boundary conditions were determined as follows. The displacement of boundary BC in lateral

Table 2: The calculation value of $\kappa_i$ at D1 section of the tunnel using equation (21).

| Date | Minimum air temperature (°C) | Maximum air temperature (°C) | Time interval (h) | $k_i$ |
|---|---|---|---|---|
| 2019/11/21 | −0.47 | 1.90 | 12 | 0.02 |
| 2019/11/22 | −0.12 | 2.50 | 8 | 0.03 |
| 2019/11/25 | −2.55 | 1.00 | 12 | 0.02 |
| 2019/11/27 | −1.05 | 2.00 | 8 | 0.03 |
| 2019/11/28 | −6.77 | 1.20 | 16 | 0.04 |
| 2020/3/7 | −2.67 | 0.80 | 8 | 0.03 |
| 2020/3/18 | −3.07 | 1.30 | 8 | 0.04 |
| 2020/3/19 | −2.45 | 0.60 | 8 | 0.03 |
| 2020/3/20 | −2.23 | 0.80 | 8 | 0.03 |
| 2020/3/22 | −1.47 | 1.70 | 8 | 0.03 |
| 2020/3/23 | −1.80 | 0.90 | 8 | 0.03 |
| 2020/3/25 | −1.08 | 2.00 | 8 | 0.03 |
| 2020/3/26 | −1.28 | 0.30 | 8 | 0.02 |
| 2020/3/27 | −0.65 | 1.80 | 8 | 0.02 |
| 2020/3/29 | −1.98 | 0.50 | 8 | 0.02 |
| 2020/3/30 | −2.35 | 0.50 | 8 | 0.03 |
| 2020/4/1 | −1.90 | 1.80 | 12 | 0.02 |
| 2020/4/2 | −3.33 | 1.20 | 8 | 0.05 |
| 2020/4/4 | −2.87 | 0.40 | 8 | 0.03 |
| 2020/4/5 | −1.53 | 2.20 | 12 | 0.02 |
| 2020/4/6 | −2.00 | 0.80 | 8 | 0.03 |
| 2020/5/7 | −1.87 | 0.30 | 8 | 0.02 |
| 2020/10/10 | −0.63 | 3.30 | 16 | 0.02 |
| 2020/10/11 | −2.02 | 1.00 | 20 | 0.01 |
| 2020/10/14 | −2.67 | 2.10 | 20 | 0.02 |
| 2020/10/15 | −3.03 | 0.50 | 16 | 0.02 |
| 2020/10/16 | −2.20 | 1.40 | 16 | 0.02 |
| 2020/10/17 | −2.43 | 0.10 | 8 | 0.03 |
| 2020/10/18 | −1.33 | 2.20 | 16 | 0.02 |
| 2020/10/22 | −0.15 | 4.00 | 16 | 0.02 |
| 2020/10/24 | −0.83 | 4.10 | 16 | 0.02 |
| 2020/10/25 | −2.63 | 0.20 | 16 | 0.01 |
| 2020/10/29 | −2.15 | 3.20 | 16 | 0.03 |
| 2020/11/2 | −2.37 | 0.40 | 16 | 0.01 |
| 2020/11/8 | −0.83 | 0.60 | 8 | 0.01 |
| 2020/11/10 | −0.65 | 2.30 | 12 | 0.02 |
| 2020/11/16 | −4.72 | 2.90 | 16 | 0.04 |

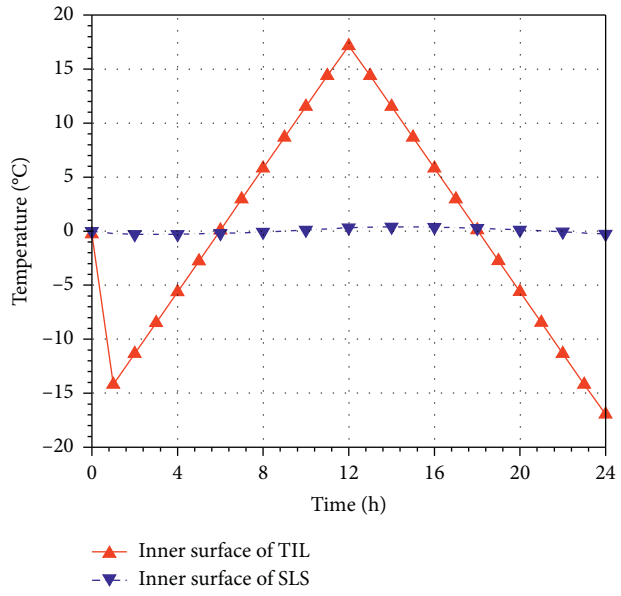


Figure 4: The variation of temperatures at inner surfaces of TIL and SLS.

Table 3: The physical parameters of lining structure and SR in numerical simulation.

| | Density (kg/m$^3$) | Elastic modulus (MPa) | Poisson's ratio | Thermal expansion coefficient (1/°C) |
|---|---|---|---|---|
| SR | 1800 | 900 | 0.3 | $5\times10^{-5}$ |
| PSL | 2500 | 2800 | 0.2 | $6\times10^{-5}$ |
| SLS | 2500 | 3000 | 0.2 | $6\times10^{-5}$ |
| TIL | 188 | 0.2 | 0.2 | $5\times10^{-5}$ |

direction was set as 0 m. The displacement of boundary CD in vertical direction was also 0 m. The boundary AD was set as symmetry boundary.

With the mathematical model including liquid water flows, heat transfer, and mechanism equation mentioned above, the frost problem could be solved by the commercial software of COMSOL Multiphysics. The spatial and temporal discretization of mathematical model and governing equations were carried out through using finite method [5]. This simulation was conducted over a time period of 50 years before the tunnel excavation to gain the initial field conditions. After the excavation, the boundary conditions were set as the ones described above.

## 5. Results and Analysis

*5.1. Long-Term Thermal and Stress Regimes at D1 of the Tunnel.* For the most tunnels in permafrost regions on the QTP, the MSFD generally occurs in mid-April. In the following analysis, the timepoint was chosen to investigate the long-term thermal regimes of the SR and stress regimes of the lining structures.

Figure 5 shows the thermal regimes at D1 in WTIL on April 15 in 5 years of the operation period of the tunnel. It can be seen that, due to the heat exchange between the air changing with the time and the lining structures, the SR close to the lining structures had a lower temperature on April 15 in 5 years of the operation period, while with the distance from the lining structures increasing, the temperature of the SR gradually rose. In the 5$^{th}$ year of the operation period, the MSFD of the SR was 1.6 m, approximately. Then, due to the geometrical shape of the tunnel, the thermal regimes of different position of the tunnel were considerably different. For example, the MSFD of the SR at the inverted arch was obviously smaller than that of the vault, while the MSFD of the SR at the foot of arch was situated between the two.

Figure 6 shows the stress regimes of the primary lining structure at D1 in WTIL on April 15 in 5 years of the operation period of the tunnel. It can be seen that both the MAPS and MIPS of the primary lining structure in cold season are bigger than those in warm season. For example, the absolute maximum value of MAPS in cold season was −3.6 MPa, while that in warm season was −2.3 MPa. Moreover, the absolute maximum value of MIPS in cold season was −1.4 MPa, while that in warm season was −1.0 MPa. The tensile stress of the primary lining structure was 0.7 MPa in cold season and 0.2 MPa in warm season. It reflected that in cold season, due to the heat exchange between the cold air and the SR, the liquid water in the SR was transferred to the solid ice leading the frost heave force loading on the primary lining structure, while in warm

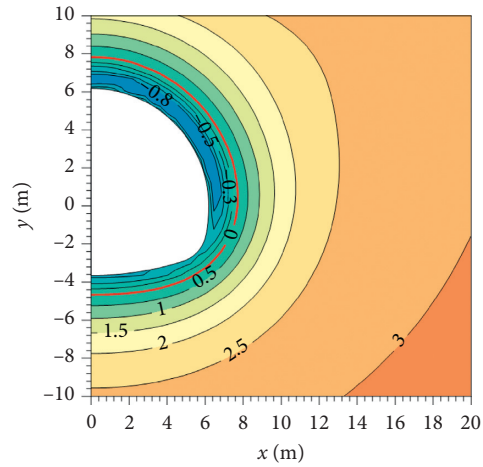


Figure 5: Thermal regimes at D1 in WTIL on April 15 in 5 years of the operation period of the tunnel.

season, there was no frost heave force surrounding the primary lining structure. Moreover, the material of the primary lining structure belonged to be the material which cannot resist too much tensile stress. Then, it was considerably essential to decrease the tensile stress related to the frost heave force on the primary lining structure.

Figure 7 shows the stress regimes of the second lining structure at D1 in WTIL on April 15 in 5 years of the operation period of the tunnel. It can be seen that the size relationship of the MAPS and MIPS of the second lining structure was generally the same as that of the primary lining structure. For example, the absolute maximum value of the MAPS of the second lining structure in cold season was −5.4 MPa, which was 0.9 MPa bigger than that in warm season. The absolute maximum value of the MIPS of the second lining structure in cold season was −2.8 MPa, which was also 1.7 MPa bigger than that in warm season. Moreover, the tensile stress in cold season was 0.8 MPa, while that in warm season was only 0.46 MPa.

The above results showed that in cold season both the absolute values of MAPS and MIPS of the primary and second lining structure were bigger than those in warm season. Moreover, both the values of tensile stress of the primary and second lining structure were bigger than those in warm season. For the lining structures of the tunnel, which cannot resist too much tensile stress, it was considerably essential to decrease the tensile stress related to the frost heave force on lining structures.

*5.2. Impacts of Insulation Laying Methods on Thermal Regimes at D1 of the Tunnel in Cold Seasons.* Figure 8 shows thermal regimes of SR at D1 in WTIL and STIL on April 15 in 5 years

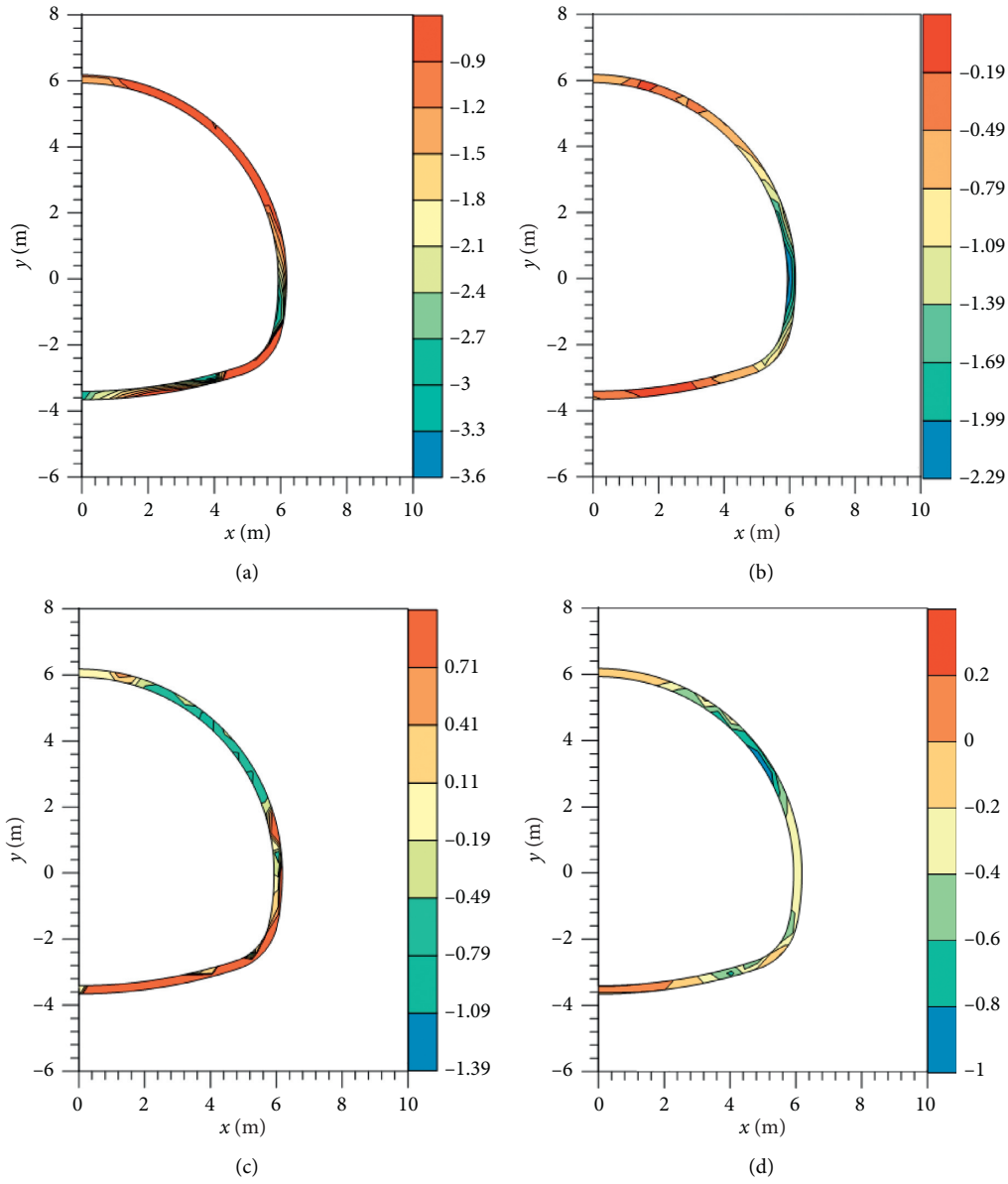


Figure 6: Stress regimes of the primary lining structure at D1 in WTIL on April 15 in 5 years of the operation period of the tunnel. (a) MAPS in cold season. (b) MAPS in warm season. (c) MIPS in cold season. (d) MIPS in warm season.

of the operation period of the tunnel. The MSFD calculated from the outer surface of the primary lining in WTIL was 1.6 m at vault of the tunnel and it was only 1.0 m at the inverted arch, while in STIL, the MSFD at vault of the tunnel was 0.1 m and it at the inverted arch was 1.0 m. The value of the MSFD can reflect the thermal effect of the heat exchange between the air inside the tunnel and the lining structure. Then, the values of MSFD at vault and inverted arch in WTIL were generally bigger than those in STIL. Moreover, although there was insulation layer laid on the surface of the lining structure, the values of MSFD at inverted arch were basically the same both in WTIL and in STIL due to the design of insulation layer. In STIL, only the lining structure above the foot of the arch was laid on the insulation layer due to the difficulties of laying below the pavement inside the tunnel.

*5.3. Impacts of Insulation Laying Methods on Stress Regimes at D1 of the Tunnel in Cold Seasons.* Figure 9 shows MAPS in STIL, MAPS in WTIL, MIPS in STIL, and MIPS in WTIL of the primary lining structure at D1 on April 15 in 5 years of the operation period of the tunnel. It can be seen that both the MAPS and MIPS of the primary lining structure in WTIL are bigger than those in STIL. For example, the absolute maximum value of MAPS in STIL was −3.6 MPa, while that in WTIL was −5.8 MPa. Moreover, the absolute maximum value of MIPS in STIL was only −1.4 MPa, while that in

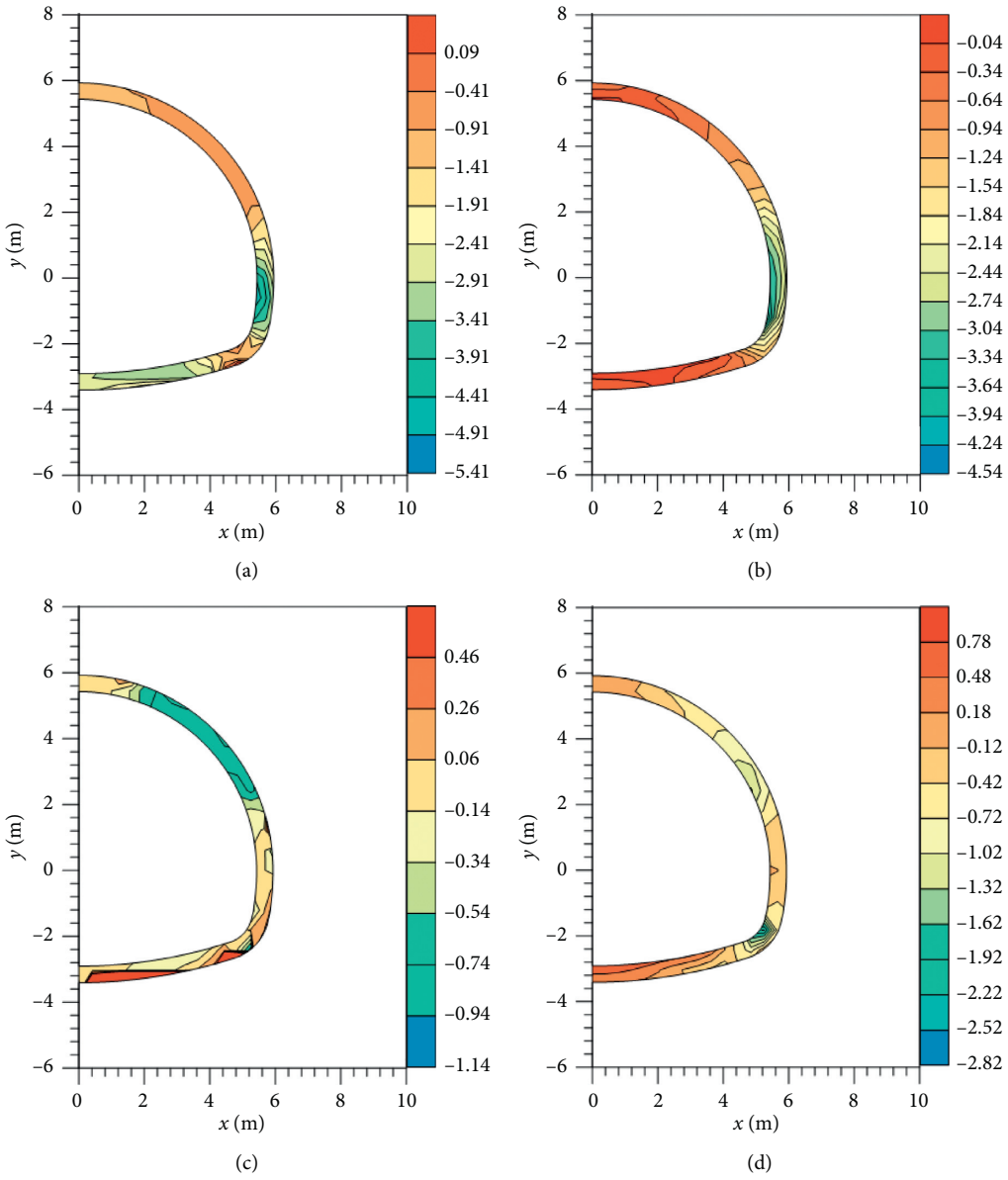


Figure 7: Stress regimes of the second lining structure at D1 in WTIL on April 15 in 5 years of the operation period of the tunnel. (a) MAPS in cold season. (b) MAPS in warm season. (c) MIPS in cold season. (d) MIPS in warm season.

WTIL was −3.0 MPa. The tensile stress of the primary lining structure was 0.7 MPa in STIL and 0.2 MPa in WTIL. It reflected that in STIL, due to the existence of the insulation layer, the thermal effect of heat exchange between the cold air and the lining structure decreased. Then, with this thermal effect, the liquid water in the SR was transferred to the solid ice leading the frost heave force loading on the primary lining structure. This meant that, in STIL, the values of the MAPS and MIPS were all smaller than those in WITL due to the existence of the insulation layer. Moreover, both the positions of the maximum absolute value of MAPS in STIL and WTIL were at the hance of the arch. The positions of the maximum tensile stress of the primary lining structure in STIL and WTIL were at the hance and inverted arch.

Figure 10 shows MAPS in STIL, MAPS in WTIL, MIPS in STIL, and MIPS in WTIL of the second lining structure at D1 on April 15 in 5 years of the operation period of the tunnel. It can be seen that both the MAPS and MIPS of the second lining structure in WTIL were bigger than those in STIL. For example, the absolute maximum value of MAPS in STIL was −5.4 MPa, while that in WTIL was −11.0 MPa. Moreover, the absolute maximum value of MIPS in STIL was only −1.1 MPa, while that in WTIL was −4.7 MPa. The tensile stress of the primary lining structure was 0.5 MPa in STIL and 2.3 MPa in WTIL. It reflected that in STIL, due to the existence of the insulation layer, the thermal effect of heat exchange between the cold air and the lining structure decreased. Then, with this thermal effect, the

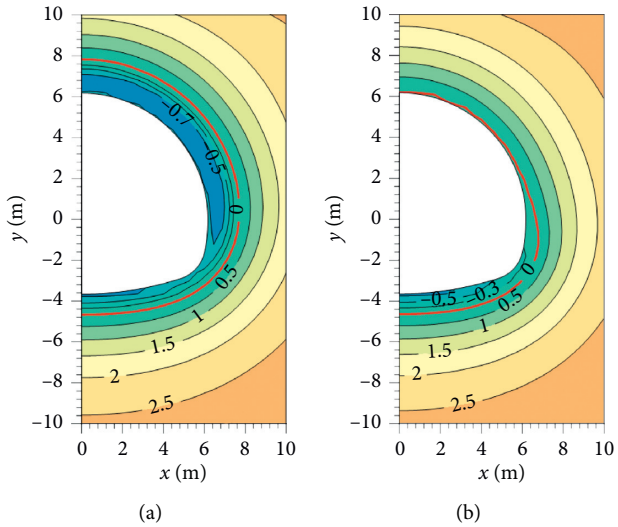


Figure 8: Thermal regimes of SR at D1 in (a) WTIL and (b) STIL on April 15 in 5 years of the operation period of the tunnel.

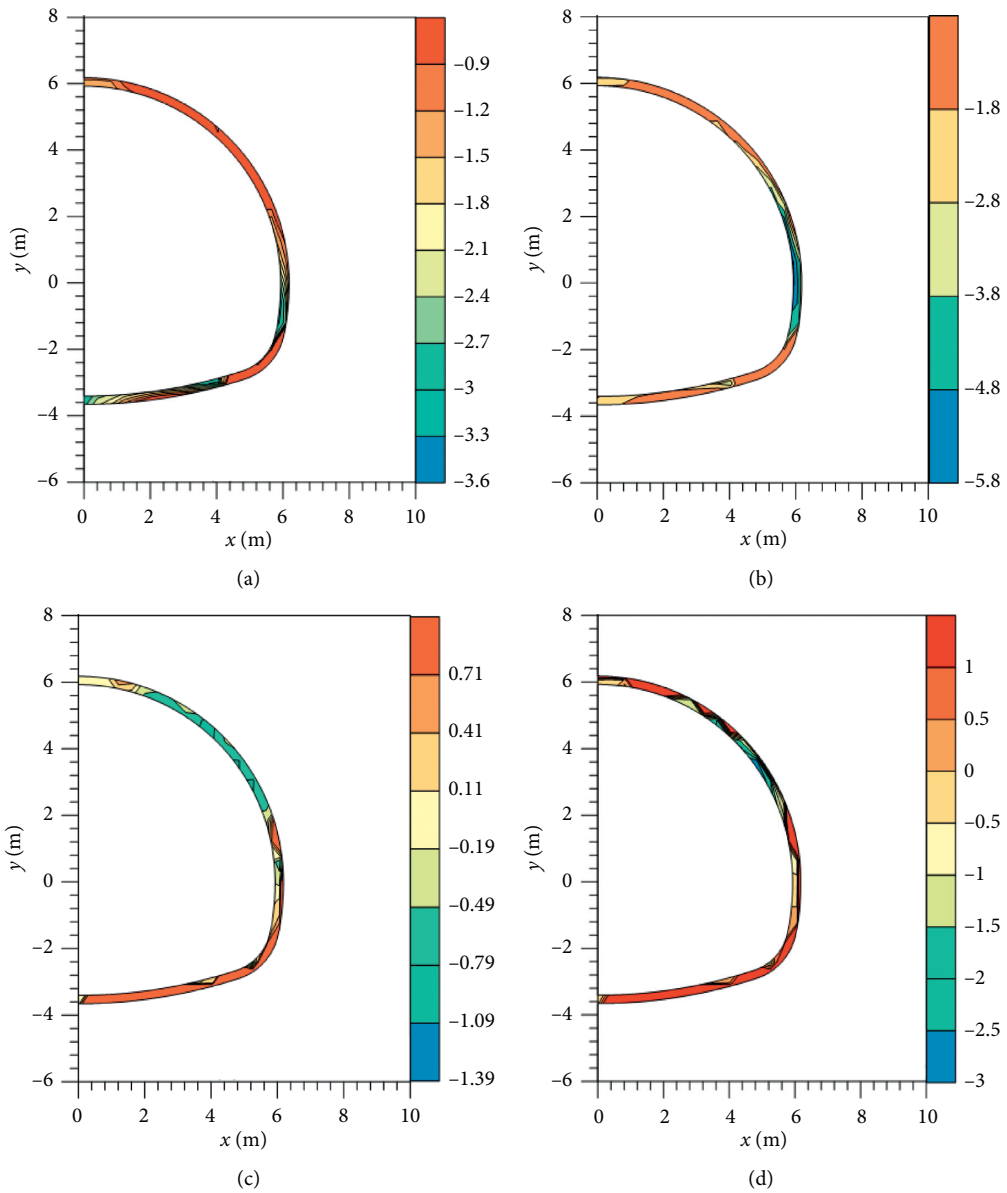


Figure 9: Stress regimes of the primary lining structure at D1 on April 15 in 5 years of the operation period of the tunnel. (a) MAPS in STIL. (b) MAPS in WTIL. (c) MIPS in STIL. (d) MIPS in WTIL.

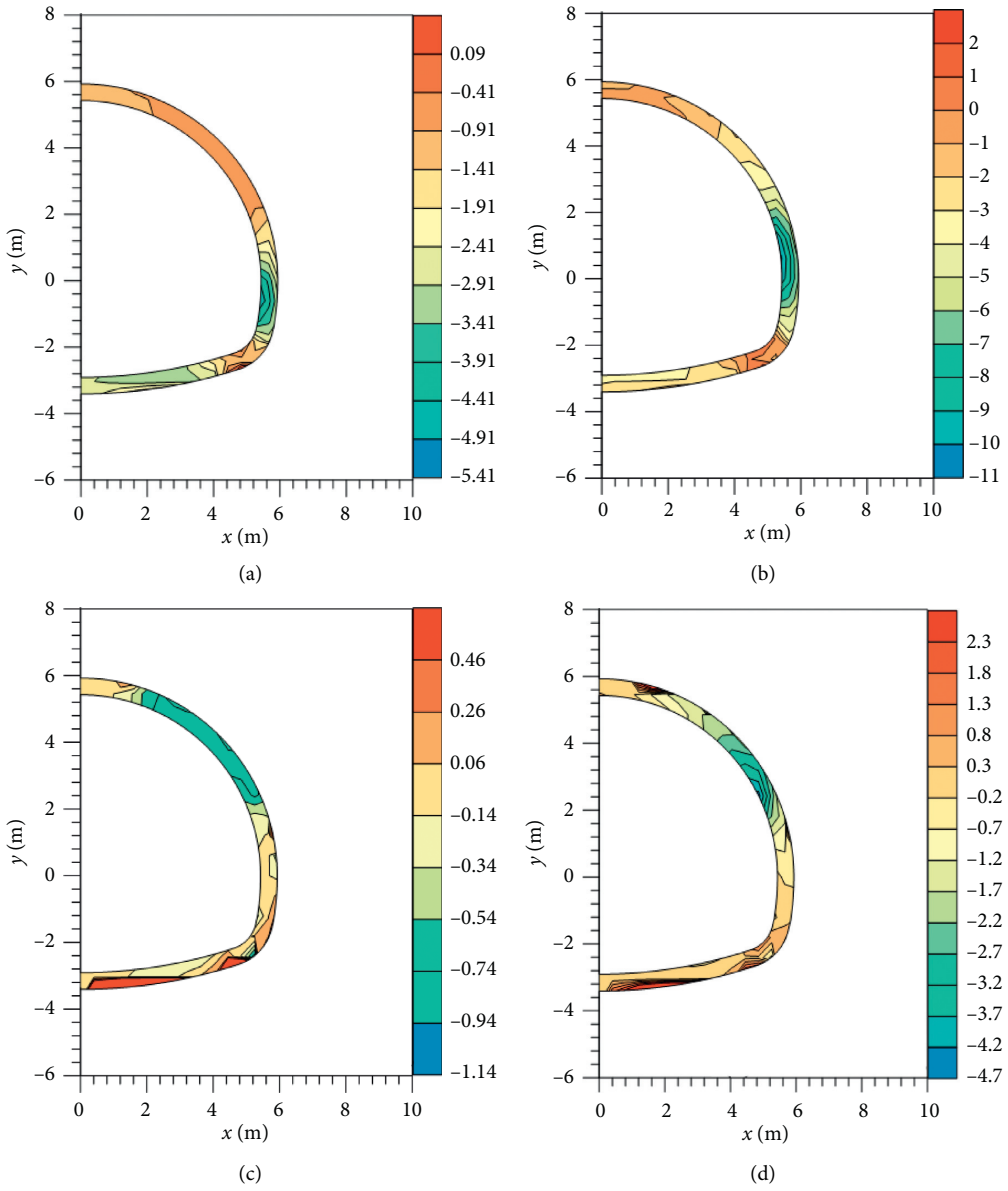


Figure 10: Stress regimes of the second lining structure at D1 on April 15 in 5 years of the operation period of the tunnel. (a) MAPS in STIL. (b) MAPS in WTIL. (c) MIPS in STIL. (d) MIPS in WTIL.

liquid water in the SR was transferred to the solid ice leading to the frost heave force loading on the primary lining structure. This meant in STIL the values of the MAPS and MIPS were all smaller than those in WITL due to the existence of the insulation layer. Moreover, both the positions of the maximum absolute value of MAPS in STIL and WTIL were at the hance of the arch. The positions of the maximum tensile stress of the primary lining structure in STIL and WTIL were at the inverted arch. For the lining structures, the greater tensile stress was generally harmful. Thus, the inverted arch of the tunnel should be laid on the insulation layer.

## 6. Conclusions

In seasonal permafrost regions, there are many frost problems of the tunnel due to the heat exchange between the air and lining structure after excavation. In this paper, a coupled mathematical model of heat, moisture transfer, and stress was constructed to investigate the long-term thermal and stress regimes of lining structures and SR of Altun highway tunnel on the QTP. Using numerical simulations, thermal and stress regimes of the tunnel in cold seasons were analyzed during a 5-year period, as well as the impact of the insulation layer methods. The conclusions were obtained as follows:

(1) In seasonally permafrost regions, there was a significant thermal disturbance of the SR after the tunnel excavation. In the 5th year of the operation period, the MSFD of the SR can reach 1.6 m at the vault of the arch. Moreover, the MSFD at the inverted arch was only 1.0 m due to the pavement inside the tunnel, while the MSFD of the SR of the foot of arch was situated between the two, which reflects that the thermal regimes of different positions of the tunnel were considerably different due to the geometrical shape of the tunnel.

(2) Both the absolute maximum value of MAPS and MIPS in cold season were bigger than those in warm season. In the 5th year of the operation period, the absolute maximum value of MAPS in cold season was −3.6 MPa, while that in warm season was −2.3 MPa. Moreover, the absolute maximum value of MIPS in cold season was −1.4 MPa, while that in warm season was −1.0 MPa. The tensile stress of the primary lining structure was 0.7 MPa in cold season and 0.2 MPa in warm season. And the law of stress regimes of primary lining structure was the same as those of the second lining structure. It reflected that in cold season, due to the heat exchange between the cold air and the SR, the liquid water in the SR was transferred to the solid ice leading to the frost heave force loading on the lining structure, while in warm season, there was no frost heave force surrounding the lining structure.

(3) Both the MAPS and MIPS of the lining structure in WTIL are bigger than those in STIL.

The absolute maximum value of MAPS of the primary lining in STIL was −3.6 MPa, while that in WTIL was −5.8 MPa. Moreover, the absolute maximum value of MIPS of primary lining in STIL was only −1.4 MPa, while that in WTIL was −3.0 MPa. The tensile stress of the primary lining structure was 0.7 MPa in STIL and 0.2 MPa in WTIL. And the law of stress regimes of primary lining structure was the same as those of the second lining structure. It reflected that in STIL, due to the existence of the insulation layer, the thermal effect of heat exchange between the cold air and the lining structure decreased, while the position of maximum value of MAPS and MIPS differs in STIL and WTIL. The positions of the maximum tensile stress of the primary lining structure in STIL and WTIL were at the hance and inverted arch, while the positions of the maximum tensile stress of the primary lining structure in STIL and WTIL were at the inverted arch. For the lining structures, the greater tensile stress was generally harmful. Thus, the inverted arch and the hance of the tunnel should be laid on the insulation layer.

## Data Availability

The data used to support the findings of this study are available from the corresponding author upon request.

## Conflicts of Interest

The authors declare that there are no conflicts of interest related to this manuscript.

## Acknowledgments

This study was supported by a research program funded by the Department of Transportation of Gansu Province (No. 2017-008).

## References

[1] X. Z. Xu, J. C. Wang, and L. X. Zhang, *Physics of Frozen Soil*, Science Press, Beijing, China, 2010.

[2] D. H. Qin, *Cryosphere Science*, Meteorological Press, Beijing, China, 2014.

[3] H. Yu, K. Zhang, X. M. Zhu, Z. Z. Tian, Y. H. Mu, and G. Q. Bi, "Numerical study on thermal insulation of a roadway tunnel at southeast edge of the Qinghai-Tibet plateau," *Earth and Environment Science*, vol. 719, Article ID 032068, 2021.

[4] K. Zhang, X. M. Zhu, H. Yu, Z. Z. Tian, Y. H. Mu, and G. Q. Bi, "Comparison thermal insulation effects of different thermal insulation materials for a roadway tunnel at southeast edge of the Qinghai-Tibet plateau," *Earth and Environment Science*, vol. 719, Article ID 032084, 2021.

[5] H. Yu, H. W. Han, W. Ma, Z. K. Ding, and L. Chen, "Long-term thermal regimes of subgrade under a drainage channel in high-altitudinal permafrost environment," *Advance in Materials Science and Engineering*, vol. 2021, Article ID 6613114, 12 pages, 2021.

[6] Y. M. Lai, M. Y. Zhang, and S. Y. Li, *Theory and Application of Cold Regions Engineering*, Science Press, Beijing, China, 2009.

[7] X. D. Bai, "Numerical calculation model of water-thermal-force coupling in tunnel section of cold area," Ph.D. Dissertation, Lanzhou Jiaotong University, Lanzhou, China, 2019.

[8] X. J. Tan, "Study on the mechanism of frost heave of tunnel in cold region with high altitude and related insulation technology," Ph.D. Dissertation, Institute of Rock and Soil Mechanics, Chinese Academy, Wuhan, China, 2010.

[9] H. Q. Xie, C. He, and Y. L. Li, "Study on insulating layer thickness by phase-change temperature field of highway tunnel in cold region," *Chinese Journal of Rock Mechanics and Engineering*, vol. 26, no. 2, pp. 4397–4440, 2007.

[10] Y. W. Zhou, D. X. Guo, and G. Q. Qiu, *Geocryology in China*, Science Press, Beijing, China, 2000.

[11] S.-b. Xie, Q. Jian-jun, L. Yuan-ming, Z. Zhi-wei, and X. Xiang-tian, "Effects of freeze-thaw cycles on soil mechanical and physical properties in the Qinghai-Tibet plateau," *Journal of Mountain Science*, vol. 12, no. 4, pp. 999–1009, 2015.

[12] G. Deng, "Investigation of frost protection design for tunnels in high altitude cold regions," Ph.D. Dissertation, Southwest Jiaotong University, Chendu, China, 2012.

[13] N. I. Johansen, S. L. Huang, and N. B. Aughenbaugh, "Alaska's CRREL permafrost tunnel," *Tunnelling and Underground Space Technology*, vol. 3, no. 1, pp. 19–24, 1988.

[14] K. Okada and Y. Matsumoto, "Actual state of frost penetration depth in railway tunnel and its analysis against periodic change of atmospheric temperature," *Doboku Gakkai Ronbunshu*, vol. 1990, no. 424, pp. 179–186, 1990.

[15] F. M. Nie, "Dynamic state of air temperature in railway tunnels in cold regions," *Journal of Glaciology and Geocryology*, vol. 10, no. 4, pp. 450–453, 1988.

[16] Y. M. Lai, Z. W. Wu, S. J. Zhang, W. B. Yu, and Y. S. Deng, "In-situ observed study for effect of heat preservation in cold regions tunnels," *Journal of the China Railway Society*, vol. 25, no. 1, pp. 81–86, 2003.

[17] R. L. Harlan, "Analysis of coupled heat-fluid transport in partially frozen soil," *Water Resources Research*, vol. 9, no. 5, pp. 1314–1323, 1973.

[18] I. Shingo, "Driving force for water migration in frozen clayey soil," *Soil Science & Plant Nutrition*, vol. 26, no. 2, pp. 215–227, 1980.

[19] G. S. Taylor and J. N. Luthin, "A model for coupled heat and moisture transfer during soil freezing," *Canadian Geotechnical Journal*, vol. 15, no. 4, pp. 548–555, 1978.

[20] S. A. Shoop and S. R. Bigl, "Moisture migration during freeze and thaw of unsaturated soils modeling and large scale experiments," *Cold Regions Science and Technology*, vol. 25, no. 1, pp. 33–45, 1997.

[21] K. Hansson, J. Simunek, M. Mizoguchi, and M. T. van Genuchten, "Water flow and heat transport in frozen soil: numerical solution and freeze-thaw applications," *Vadose Zone Journal*, vol. 3, pp. 693–704, 2004.

[22] Y. M. Lai, Z. W. Wu, Y. L. Zhu, C. X. He, and L. N. Zhu, "Nonlinear analysis for the coupled problem of temperature and seepage fields in cold regions tunnels," *Science in China, Series D*, vol. 29, no. 1, pp. 89–96, 1999.

[23] X. F. Zhang, Y. M. Lai, W. B. Yu, and S. J. Zhang, "Non-linear analysis for the freezing-thawing situation of the rock surrounding the tunnel in cold regions under the conditions of different construction seasons, initial temperatures and insulations," *Tunnelling and Underground Space Technology*, vol. 17, no. 3, pp. 315–325, 2002.

[24] X. J. Tan, W. Z. Chen, D. S. Yang et al., "Study on the influence of airflow on the temperature of the surrounding rock in a cold region tunnel and its application to insulation layer design," *Applied Thermal Engineering*, vol. 67, no. 1-2, pp. 320–334, 2014.

[25] Y. F. Zhou, X. F. Zhang, and J. H. Deng, "A mathematical optimization model of insulation layer's parameters in seasonally frozen tunnel engineering," *Cold Regions Science and Technology*, vol. 101, pp. 73–80, 2014.

[26] Q. G. Ma, X. X. Luo, Y. M. Lai, F. J. Niu, and J. Q. Hao, "Numerical investigation on thermal insulation layer of a tunnel in seasonally frozen regions," *Applied Thermal Engineering*, vol. 138, pp. 280–291, 2018.

[27] W. W. Liu, Q. Feng, C. Wang, C. K. Lu, Z. Z. Xu, and W. T. Li, "Analytical solution for three-dimensional radial heat transfer in a cold-region tunnel," *Cold Regions Science and Technology*, vol. 164, Article ID 102787, 2019.

[28] J. M. Zhang, "Study on roadbed stability in permafrost regions on Qinghai-Tibetan plateau and classification of permafrost in highway engineering," Ph.D. Dissertation, University of Chinese Academy of Sciences, Lanzhou, China, 2004.

[29] M. L. Zhang, Z. Wen, K. Xue, L. Z. Chen, and D. S. Li, "A coupled model for liquid water, water vapor and heat transport of saturated-unsaturated soil in cold regions: model formulation and verification," *Environmental Earth Sciences*, vol. 75, no. 8, pp. 1–19, 2016.

[30] M. T. van Genuchten, "A closed-form equation for predicting the hydraulic conductivity of unsaturated soils," *Soil Science Society of America Journal*, vol. 44, no. 5, pp. 892–898, 1980.

[31] Y. Mualem, "A new model for predicting the hydraulic conductivity of unsaturated porous media," *Water Resources Research*, vol. 12, no. 3, pp. 513–522, 1976.

[32] H. P. Hu, S. X. Yang, and Z. D. Lei, "A numerical simulation for heat and moisture transfer during soil freezing," *Journal of Hydraulic Engineering*, vol. 7, pp. 1–8, 1992.

[33] Z. W. Zhu, J. G. Ning, and W. Ma, "Study on a constitutive model of frozen soil based on damage and moisture-thermal-mechanism numerical simulation," *Scientia Sinica*, vol. 40, no. 6, pp. 758–772, 2010.

[34] Y. X. Xia and Y. D. Wang, *Mechanical Calculation of Tunnel Structure*, People's Communications Press, Beijing, China, 2001.

[35] X. L. Liu and G. P. Tang, "Research on prediction method of concrete freeze-thaw durability under field environments," *Chinese Journal of Rock Mechanics and Engineering*, vol. 26, no. 12, pp. 2412–2419, 2007.

[36] H. Cao, W. Z. Tan, and X. L. Liu, "Loss of mechanical properties of concrete under freeze-thaw cycles," in *Proceedings of the 5th National Structural Engineering Academic Conference*, Chicago, IL, USA, 1996.

[37] H. Cai, "Prediction model of frost resistance durability of concrete," Ph.D. Dissertation, Tsinghua University, Beijing, China, 1998.

[38] R. X. He, H. J. Jin, S. P. Zhao, and Y. S. Deng, "Review of status and progress of the study in thermal conductivity of frozen soil," *Journal of Glaciology and Geocryology*, vol. 40, no. 1, pp. 116–126, 2018.